ELSEVIER

Contents lists available at ScienceDirect

# Journal of Magnetism and Magnetic Materials

journal homepage: www.elsevier.com/locate/jmmm





# Particle organization versus volume fraction in magneto-active elastomer composites

Tyler Haussener, Niknam Momenzadeh\*, Paris von Lockette

Department of Mechanical Engineering, The Pennsylvania State University, State College, PA 16802, USA

#### ARTICLE INFO

Keywords:
Magneto-active elastomers
Smart materials
Barium ferrite
X-ray diffraction
Vibrating sample magnetometry

#### ABSTRACT

Magneto-active elastomers (MAEs) are a subclass of smart materials that have the ability to actuate and alter their mechanical and magnetic response when subjected to an external magnetic field. Past research has shown that higher net magnetic remanence of an MAE is desirable to increase actuation and produce the most magnetic work. To create a magnetically aligned MAE, a hard magnetic material is mixed in an elastomer solution, then cured in a strong external magnetic field causing particle alignment. A high degree of alignment of magnetic particles is expected to result in improved remanence. However, in MAEs with soft magnetic particles cured in a field, past research has shown that the degree of alignment, vs. less ordered clustering, varies with particulate volume content. Consequently, it is important to study the degree to which volume content of magnetic material affects physical particle alignment, bulk magnetic properties, and the coupling between the two in MAEs with hard magnetic filler particles. In this study MAEs with a hard magnetic filer (barium ferrite) are investigated with varying volume content of magnetic material ranging from 5 to 30% by volume. Batches of MAEs were tested using X-ray diffraction and vibrating sample magnetometry to gain information on crystal structure and bulk magnetic properties. The results of the collected data suggested all poled samples had both higher physical particle orientation as well as a larger remanence than the unpoled counterparts. As volume fraction of magnetic filler was increased the net magnetic properties per volume of magnetic material remained fairly constant. However, the degree of physical particle orientation varied with a local minimum at medium volume fractions. Collected data was used to calculate two orientation parameters, the degree of preferred alignment parameter,  $\eta$ , and the orientation of distributions of magnetic domains parameter,  $\sigma$ . The two parameters were compared to show a relationship between physical particle alignment and net magnetic properties as volume of magnetic material increases. Based on the collected results, a hypothesis is presented on how particle interaction is speculated to evolve as volume fraction of magnetic material is increased.

#### 1. Introduction

Magneto-active elastomers (MAEs) are a subclass of a more well-known material, magneto-rheological elastomers (MREs). Broadly speaking, MREs are a viscoelastic solid whose mechanical properties can be controlled by an external magnetic field [1]. These composites have applications in media data storage, magnetic position sensors, flexible magnets, touch screen displays, electromagnetic shielding, vibration absorbers, and engine mounts [2–6]. When placed in an external magnetic field, the combination of internal particle interactions and the applied field leads to actuation and alteration of the material mechanical properties [7,8]. By increasing the volume content of magnetic material in an MAE the net magnetization can be increased thus increasing the

work that is able to be produced. However, previous studies have shown that increasing the amount of magnetic material causes particle interactions to occur that may limit the bulk magnetic properties of the MAE[9].

Various magnetic fillers have been used in MAEs to maximize actuation. Previous work has investigated the behavior between materials embedded with hard magnetic materials (barium ferrite) in two cases: aligned, or materials cured in a high magnetic field and unaligned, or materials cured in zero field[10]. Results showed the combination of hard magnetic particles and coherent alignment of the particles' magnetizations were required to maximize actuation. It has also been shown that hard magnetic materials with higher net magnetizations produce larger motion and blocked forces[11].

E-mail address: Nmm6089@psu.edu (N. Momenzadeh).

<sup>\*</sup> Corresponding author.

Based on the results of the previous work, hard magnetic barium ferrite (BaFe) is chosen as the magnetic filler of the MAEs in this study. Due to its hexagonal magnetoplumbite structure the material is referred to as barium hexaferrite as well. It is attractive to MAE applications due to its relatively high Curie temperature of 450 °C, high coercive force of 6700 Oe, high magnetic anisotropy field, and its chemical stability to resist corrosion[12-14]. Its high anisotropic magnetic field indicates that the coherent alignment of particles can create a greater bulk magnetic moment. Due to the size and shape of barium particles, typical barium ferrite crystals grow very little in its crystallographic c-direction while growth is significantly more rapid in the crystallographic a-plane. This growth causes barium ferrite to form thin hexagonal plate-like structures with the easy axis of magnetization out of plane of the plates[15]. These structures result in anisotropic magnetic properties within a crystal[16]. The alignment of BaM particles in a magnetic field is directly related to its crystallographic orientation since the easy axis of magnetization corresponds to the crystallographic c-axis[17]. In a bulk sample of BaM, randomly oriented particles result in isotropic magnetic behavior. Therefore, to achieve the most efficient development of anisotropic magnetic performance it is desirable to magnetically align the particles of BaM within a given sample.

In MAE applications, samples may be poled in various directions causing hard magnetic particles to align within the sample in various orientations. Two of the most common directions of poling are in-plane and out-of-plane. These alignment directions are shown in Fig. 1 where the bulk gray cylinder represents the elastomer matrix, the large blue arrow points in the direction of the applied field, and the small black arrows represent the hard magnetic particles pointing in the direction of their internal magnetization.

Previous work has quantified the magnetic properties of both barium ferrite powders and MAEs containing various weight percentages of barium by collecting hysteresis loops of samples[12,18,19]. Results showed that increasing the barium ferrite content in a Polyvinylidene fluoride (PVDF) material increases both remanent and saturation magnetization[19]. Previous work has also investigated the change in particle microstructure as volume content of magnetic material (iron) is increased[9]. Results showed lower fractions (1.5 and 11.5% by volume) contained well-ordered chainlike structures which had larger spatial separation between particles. Higher volume fractions (33% by volume) showed more complex clusters of particles with less spatial separation between them. The transformation from well-ordered structures to particle clusters may limit the bulk magnetic properties of the MAE. While previous studies have measured the bulk magnetic properties and microstructure of MAEs with varied volume content of magnetic material, studies have not linked the physical assessment of particle orientation to bulk magnetic properties as this study purposes.

By measuring the hysteresis curve for samples, remanent and saturation magnetization can be extracted. By determining these values, it is possible to quantify the distribution of internal magnetic domains in an MAE. Previous work has related the squareness ratio, or the ratio of measured remanent magnetization to the saturation magnetization to the distribution of orientations of magnetic domains in an MAE[20]. Details are given in Appendix C. By considering a single magnetic domain in a Cartesian coordinate system, the location and orientation of the domain can be completely described. Integrating over the entire sample volume in the coordinate system and assuming a Gaussian distribution of magnetic domains, the width of the distribution,  $\sigma$ , can be determined. Ideally samples with a high degree of magnetic alignment will have a narrow distribution and show small  $\sigma$  values. Randomly

orientated domains will show a broad distribution of magnetic domains indicated by a large  $\sigma$ .

In order to determine the degree of physical particle alignment in an MAE, X-ray diffraction (XRD) techniques can be applied. Previous work has theoretically calculated and experimentally confirmed the lattice spacing associated with each (hkl) plane in barium ferrite[21]. This theoretical pattern represents the random orientation of barium ferrite, or how the material would naturally appear before any alterations are made to crystallinity or structure [22]. Using this reference pattern allows for the comparison of peak intensities as well as match Miller indices to the correct peaks in the pattern. Previous studies have used techniques to determine physical particle alignment in samples [23]. By collecting the XRD pattern for samples the appropriate crystallographic planes, and thus peak intensities, in the pattern can be compared to determine if particles are aligned with preferred alignment in the observed planes. However, the direct comparison of absolute peak intensities from sample to sample cannot be done. Many factors affect the intensity of diffracted x-rays from a sample between two runs. Sample placement, sample size, sample height, temperature, and the tube strength from the source of x-rays all have an impact of the absolute intensity of x-rays diffracted [24]. For this reason, it is important to compare relative intensities between samples, or the ratio of absolute intensities of a given plane to another plane in the material [24]. In XRD it is typical to define relative intensities to the maximum peak in the pattern such that the maximum peak has a relative intensity of one and each other peak in the pattern has a relative intensity less than one.

Using collected XRD patterns, previous work by Zolotoyabko has developed an analytical method to quantify the degree of preferred orientation of crystallites [25]. First the collected relative intensities  $I(\boldsymbol{h})$  and  $I(\boldsymbol{h}_0)$ , along an arbitrary axis ,  $\boldsymbol{h}$ , and the nominal alignment axis,  $\boldsymbol{h}_0$ , are related to the corresponding relative intensity of the powder pattern to define the March parameter,  $\boldsymbol{r}$ , from

$$r = \left[\frac{\sin^3(\alpha)}{\left(\frac{\kappa}{\kappa_p}\right)^{2/3} - \cos^2(\alpha)}\right]^{1/3}$$
 (1)

Here,  $\kappa = I(h_0)/I(h)$ ,  $\alpha$  is the angle between h and  $h_0$ , and  $\kappa_p = I(h_0)/I(h_\infty)$  where  $I(h_\infty)$  is the intensity of a random powder sample. The degree of preferred orientation of crystallites,  $\eta$ , can then be calculated as a function of r from

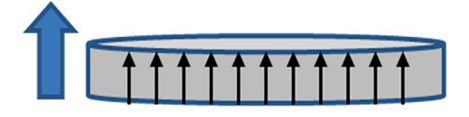
$$\eta(\%) = \left[ \frac{(1-r)^3}{1-r^3} \right]^{\frac{1}{2}} \times 100 \tag{2}$$

where the  $\eta$  parameter is defined as 100% for the case of perfect uniaxial preferred orientation, and 0% for a perfectly random powder.

# 2. Material and methods

# 2.1. Morphology of the fabricated samples

The MAEs used in this study were fabricated using a silicone rubber compound and Barium ferrite (BaFe). Barium ferrite with the chemical formula BaFe $_{12}O_{19}$  is also referred to as M-type barium hexaferrite (BaM). The barium ferrite used in this study was 325 mesh (particle size less than 44 µm) < BaFe $_{12}O_{19}$  > of 99.9% purity from ESPI metals (ESPI Metals, Oregon, USA, stock number: Knc6220). A silicone solution of DOW Sylgard 184 rubber compound was mixed with its catalyst at a



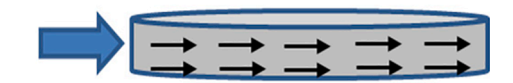


Fig. 1. Illustration of hard magnetic particles in an MRE poled out-of-plane (left) and in-plane (right). Arrows represent the preferred magnetic axis of a particle.

10:1 ratio in an aluminum mixing pan. To be sure the silicone and catalyst compound were not degraded, all samples were made using solution that had not been opened for more than one month. The catalyst and silicone mixture were mixed together by hand using a spatula micro spoon for at least 5 min. After the catalyst and silicone solution was well mixed, the required mass of BaM to achieve a desired volume fraction was added by

$$M_B = \frac{\%vol}{(1 - \%vol)} \frac{\rho_{Barium}}{\rho_{elastomer}} M_{elast/cat}$$
(8)

where *%vol* is the desired volume fraction of BaM in the MAE,  $\rho$  is the density of barium or elastomer as listed, and  $M_{elast/cat}$  is the mass of the elastomer/catalyst solution. The density of the 325 mesh BaM used in this study is  $5.28\frac{R}{cm^3}$ , and the density of the elastomer used is  $1.00\frac{R}{cm^3}$ .

The mixture was mechanically mixed after each addition. The mixture was then placed in acrylic molds to cast the MAEs as cylinders with a diameter of 6 mm and height of 1.5 mm. Enough solution was mixed to cast four samples in two identical molds. One of the molds was set aside for at least two days to cure outside of the influence of a magnetic field. These samples are referred to as the unpoled samples for a given volume fraction. The second set of samples in the second mold were immediately placed in a MFG-6–12 Magnetech Corp table top magnet with the poling faces sitting directly in contact with the top and bottom of the mold. This poling configuration is shown in Fig. 2.

Samples were subjected to an applied field of 1.43 T for about 12 min, or until the poling magnet reached a maximum temperature of 50  $^{\circ}$ C. By placing the mold between the poling faces as shown in Fig. 2, the magnetic flux lines of the electromagnet were perpendicular to the material being cast in the mold. This configuration poled all the MAEs in this study out-of-plane. All poled samples were left to cool in the poling magnetic for at least 12 h before removing them from the mold.

Batches of MAEs were fabricated with 5%, 10%, 15%, 20%, 25%, and 30% by volume BaM. Each batch contained four poled and four unpoled samples. The same BaM-elastomer mixture was used to cast both poled and unpoled samples of each volume fraction for consistency.

When samples are poled, the coherent alignment of BaM particles increases the bulk magnetic remanence of a sample. The alignment of the physical particles can be seen by scanning electron microscopy (SEM). As previously stated, particles form hexagonal plate like structures with their crystallographic c-axis, which corresponds to the easy axis of magnetization, out of plane of the plate. Therefore, it is expected to observe the plate like formations to orient with their surface normal being parallel to the applied field. These structures and their orientation

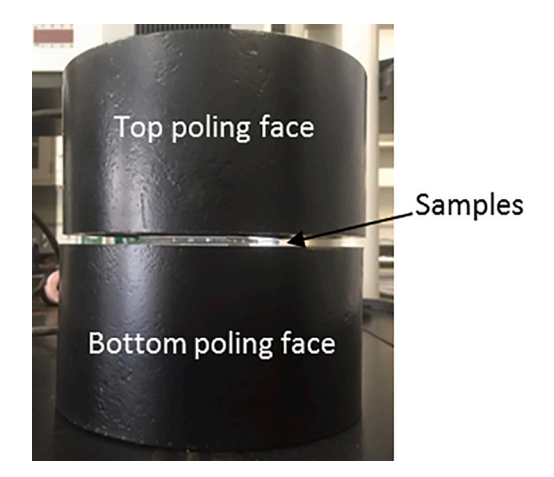


**Fig. 2.** Electromagnet used to create the poled samples. The three-part mold was placed on the bottom poling face and the top poling face rested directly on the three-part mold to maximize the magnetic field experienced by the samples by reducing the gap. The maximum field produced in this configuration was 1.43 T.

are shown by the SEM images in Fig. 3 where the white arrow corresponds to the direction of the applied magnetic field.

#### 2.2. Vibrating sample magnetometry (VSM)

Hysteresis loops were collected on all four samples in each poled batch and the four unpoled samples in the 10% by volume batch using a Microsense EZ7 vibrating sample magnetometer. Plots for each sample were measured using an applied magnetic field strength from -19500 to  $19,\!500$  Oersted (Oe). Data points were collected every 1000 Oe when the applied field was between 9500 and 19,500 Oe, and also when the applied field ranged from -19500 to -9500 Oe. When the applied field ranged between -9500 and 9500 Oe, data points were collected at 500 Oe intervals to gain higher resolution in the remanent region.

The measured magnetic moment from each of the four samples in a batch was averaged and a standard deviation was calculated for each data point collected at the applied field strengths. Fig. 4 shows the average measured magnetic moment of each batch of a given volume fraction of BaM with error bars of one standard deviation (some error bars are not visible due to the very low scatter between samples measured). As shown, the 5% and 10% by volume poled samples approach full saturation. Higher volume fractions are nearly saturated; these volume fractions, however, are experiencing coherent domain rotation as opposed to domain switching near hysteresis. For this work, we denote the highest recorded magnetization in each VSM test as the "highest magnetization". As expected, both remanence and magnitude of hysteresis increase with magnetic volume content. This trend agrees with the previous study on barium ferrite films with increasing barium ferrite content [18]. The unpoled batch shows a very low remanence, as expected since it represents an isotropic sample in which magnetic particles have no preferred orientation.

In order to compare the measured bulk magnetic moment between various volume fractions, it is necessary to normalize by the volume of magnetic material in the sample. The measured data in emu/g was normalized by the amount of magnetic material in a given sample and converted to units of Tesla. The normalized remanent and highest magnetization values (approaching saturation) from the four samples of each batch were averaged together and a standard deviation was calculated for each batch to observe trends in bulk sample magnetization. The results are shown in Fig. 5. For a baseline comparison, the average normalized remanent and highest magnetization of the 10% by volume unpoled batch tested is shown on the plot as a square marker. Since the unpoled sample ideally represents the isotropic case, the value is extended, for visual reference, across volume fractions.

According to Fig. 5, the results show a nearly constant normalized remanent value for each batch. All poled batches are within a 0.111 T (v/v) band from the calculated average normalized remanent magnetization. The maximum average remanent magnetization was shown in the 5% by volume batch with a remanence of 0.523 T (v/v), 19.7% above the mean for all volume fractions. The minimum average remanent magnetization was the 20% by volume batch with an average remanence of 0.413 T (v/v), 5.58% below the mean for all volume fractions. It can also be noted that samples showed very consistent results within each batch shown by the small standard deviation bars. For batches containing 15% BaM by volume or higher, most error bars are not visible due to the width of the data point.

The highest magnetization of each batch is very close to the average highest value for the unpoled batch. The 10% by volume unpoled batch showed a normalized highest magnetization of 0.517 T (v/v). The average highest magnetization of all poled samples for all volume fractions is 0.519 T (v/v) with a standard deviation of 6.4% from the mean. The maximum average highest magnetization measured was 0.597 T (v/v) in the 5% by volume batch, and the minimum average measured was 0.496 T (v/v) in the 30% by volume batch. This high degree of consistency for varied volume fractions is contributed to the fact that each sample used the same material, BaM, as a magnetic filler.

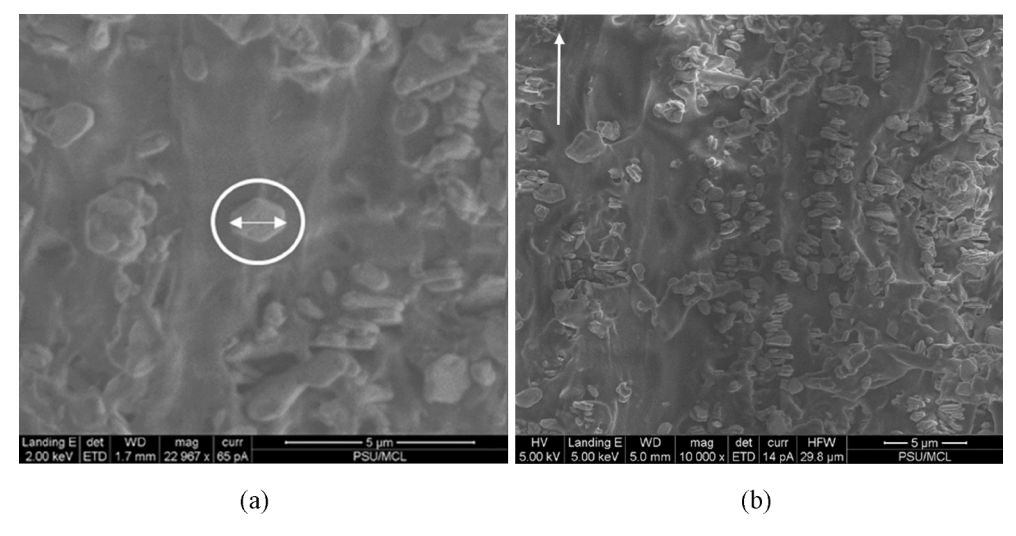


Fig. 3. (a) SEM image of a BaM plate like particle in an MAE. The structure shown in this image measures 1.46 μm from edge to edge [unpoled sample]. (b) SEM image of BaM particles in an MAE. White arrow indicates the direction of poling [poled sample].

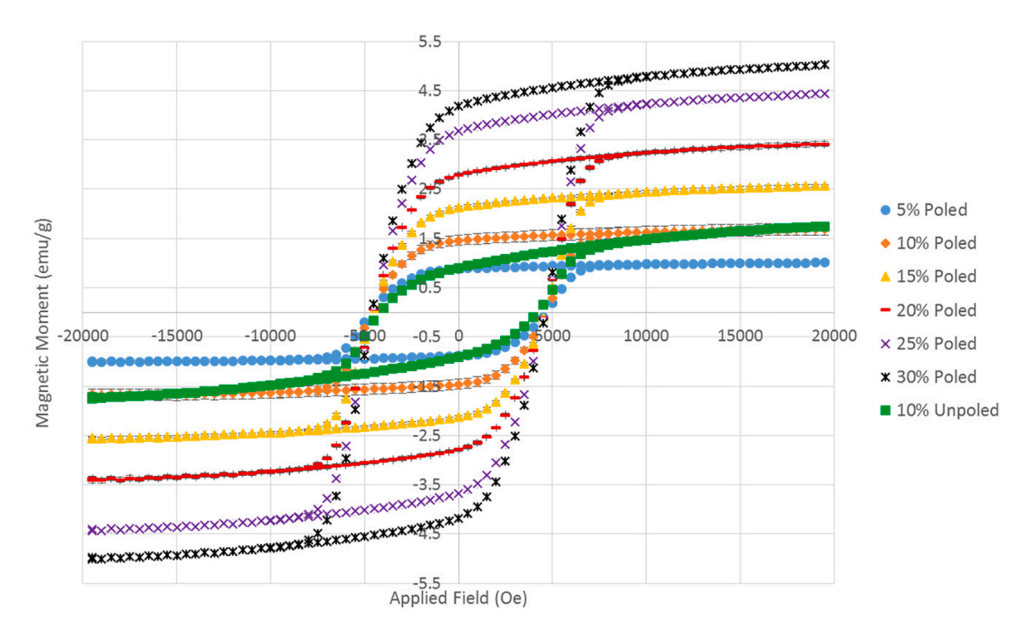


Fig. 4. Magnetic Hysteresis plot of average data points measured for all four samples per batch. Standard deviation bars are shown on each point, many are not visible due to the very small variance between samples.

The distribution of orientations of magnetic domains parameter,  $\sigma$ , was estimated for each sample using the collected VSM data. To calculate the squareness value of each sample, the measured remanent magnetization (normalized by the amount of magnetic material) was divided by the highest measured magnetization across all samples (also normalized by its amount of magnetic material). This highest measured value was 0.623 T [19]. The squareness of each sample was then related to the distribution of orientations of magnetic domains in the sample using the relationships developed in previous work [20]. An average  $\sigma$  value was then calculated for each poled batch along with the standard deviation, the results are shown in Fig. 6. A distribution parameter was only calculated for poled samples since the squareness value determined for unpoled samples was too low to mathematically calculate a  $\sigma$  value.

A small  $\sigma$  indicates a narrow distribution of magnetic domains. As shown in Fig. 6, the 5% by volume batch of samples has the smallest distribution parameter and therefore the smallest distribution of magnetic domains. Samples with 10% up to 30% by volume show a fairly uniform distribution parameter. Average  $\sigma$  values for samples between

10% and 30% volume fraction range between a minimum of 0.664 at 25% and a maximum of 0.750 at 20% by volume. The results suggest low volume fractions have a narrowly distributed distribution of magnetic domains, and higher volume fractions tend to have a more uniform (wider) distribution of magnetic domains.

By plotting the average calculated  $\sigma$  versus the average squareness of each batch correlations can be observed. The results are shown in Fig. 7.

Fig. 7 shows a linear relationship between  $\sigma$  and normalized remanent magnetization. For the greatest MAE performance, it is desired to operate in the lower right corner of the plot. This region corresponds to a narrow distribution of magnetic domains and a high remanence magnetization. As shown in the figure, the lowest volume fraction, 5% by volume, shows the highest correlation yielding a high remanence magnetization and narrow distribution of magnetic domains. The remaining five batches with varied volume fraction show inconsistent results varied with increased magnetic content. Although the data seems to form a linear trend between the orientation parameter and normalized remanence, there is no obvious trend showing a relationship to

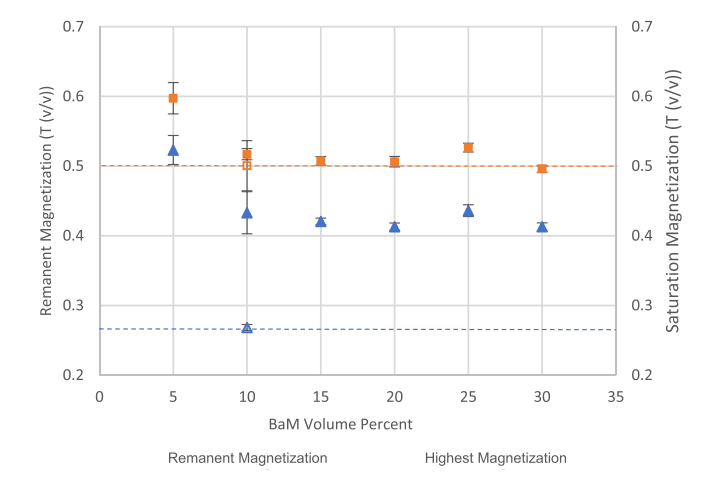


**Fig. 5.** Average normalized remanent magnetization values and average highest achieved magnetization values for each batch of poled samples with error bars of one standard deviation. The hollow marker at 10% by volume, extended across volume fractions for reference, is the average value collected from the unpoled 10% samples, and therefore represents the isotropic case.

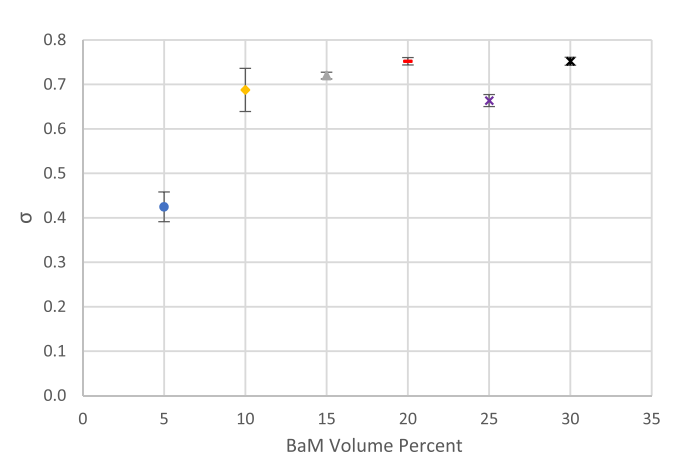
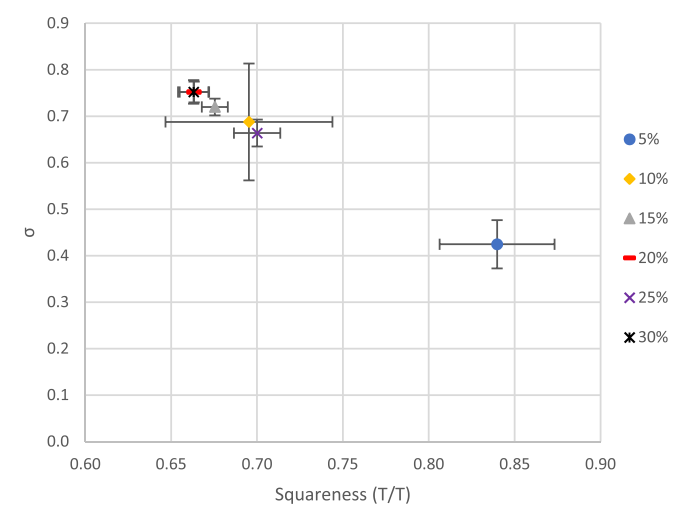


Fig. 6. Average calculated  $\sigma$  value for each batch of poled samples. Each data point is plotted with error bars of one standard deviation.



**Fig. 7.** Average calculated distribution parameter,  $\sigma$ , versus average squareness. Each data point represents a given batch, and the attached error bars show standard deviation of the batch.

increased BaM volume content. The assertion can be made that higher remanent magnetization requires a more narrow distribution of magnetic domains. The linear behavior shown above is unexpected since the  $\sigma$  parameter is determined based on a Gaussian distribution, which is an exponential function. Therefore, it is expected to observe an exponential relationship between the parameters plotted. However, the data collected may only cover a narrow band of the entire curve making it appear linear.

#### 2.3. X-ray diffraction (XRD)

X-ray diffraction pattern of each sample was measured using a PANalytical X'Pert Pro Multi-Purpose Diffractometer (MPD). Power was set to 45 kV and 40 mA to create  $\text{CuK}_{\alpha}$  radiation with a wavelength of 1.5418 Å. A beam mask of 10 mm and a scatter slit of 0.5° was used to direct the beam. Samples were tested sweeping angles from 5.0° to 70.0° in 0.0263° increments. The raw collected x-ray patterns were analyzed using Jade software. Typical diffraction patterns for a poled and unpoled MAE are shown in Fig. 8.

This study focuses on five particular Miller indices: (006), (008), (107), (114), and (0014). Since each sample was poled out-of-plane, and it is known the easy axis of magnetization corresponds with the crystallographic c-axis of BaM, the (001) directions were selected. Poling samples out-of-plane aligns the BaM particles in this direction with respect to the sample surface. The (107) plane was selected because it was found to be the maximum peak in all poled samples. The (114) plane was chosen because it is known to be the primary peak or maximum plane in a random sample; this was also proven true in all unpoled samples [21]. Since the (114) was shown to be maximum in unpoled samples and in the powder pattern [21], it was chosen as the characterization peak for relative intensities.

The relative intensity to the (114) peak of each plane of interest was recorded for every sample. An average and standard deviation was then calculated for each plane of interest of each volume fraction for both poled and unpoled batches. The results are shown in Fig. 9. Also, Table 1 shows 80 percent confidence window relative intensity of each plane of interest for every batch of samples.

The results show all planes in the direction of poling,  $(00\ 1)$  planes, and the (107) plane have a significant increase in average relative intensity for poled samples over that of unpoled samples indicating an increase of particle alignment. Also, since each of the planes of interest for every poled sample has a relative intensity above one, each of these planes have a larger absolute intensity than the (114) plane in their respective patterns. In unpoled samples, the (114) plane has the largest absolute peak intensity indicated by each of the other planes of interest having a relative intensity below one. The figure also shows that the (107) plane has a larger relative intensity than each of the other planes of interest for poled samples. In the poled batches, the average (107) relative intensity remains larger in each batch except for the 30% by volume batch. In general, comparing (hkl) planes, the average relative intensities for all volume fractions of poled samples are ranked (107), (008), (006), and (0014) from highest to lowest.

Using the relative intensity data collected in each x-ray diffraction pattern, the average degree of preferred orientation value,  $\eta$ , was calculated for each of the four poled and four unpoled samples of each volume fraction for the (006), (008), (107) and (0 0 14) planes. An  $\eta$  value cannot be defined for the (114) plane since it is the characteristic normalization plane. An  $\eta$  value of 0% indicates a perfectly random sample, and an  $\eta$  value of 100% indicates perfect uniaxial alignment.

The calculated orientation parameter suggests the unpoled batches show a low and constant degree of alignment in each plane when compared to the poled batches. Every poled volume fraction shows a higher degree of preferred orientation in each plane than the corresponding unpoled volume fraction. Among poled samples the lowest volume fraction, 5% by volume, has the highest degree of preferred alignment. There is a local minimum value in the alignment parameter

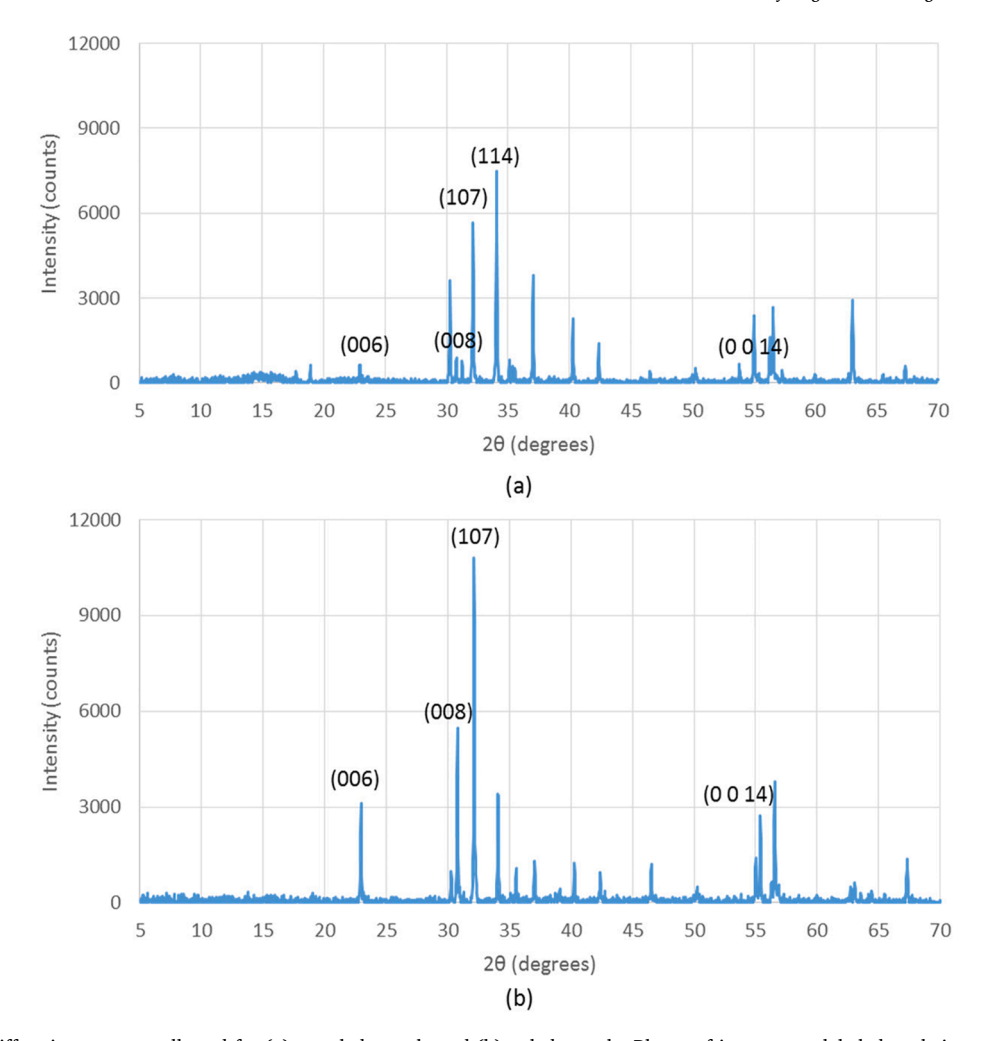


Fig. 8. Typical x-ray diffraction pattern collected for (a) unpoled sample and (b) poled sample. Planes of interest are labeled to their corresponding peaks. Both patterns shown were collected on 10% by volume BaM MAEs.

for the 15% by volume batch. As volume content increases or decreases from this local minimum the degree of preferred orientation parameter increases in each (00 l) direction.

## 2.4. Comparison of physical and magnetic alignment

To observe a correlation between particle alignment described by the calculated alignment parameter,  $\eta,$  and the bulk magnetization of a batch, the squareness was plotted versus  $\eta$  in Fig. 11. For the most efficient MAE performance, ideally each data point would be located in the upper right corner of each plot in Fig. 11. The upper right corner corresponds to a high remanent magnetization and a high degree of particle alignment. All three index planes plotted show consistent results. The 5% and 10% by volume batches are located at a higher  $\eta$  and remanence than other batches for each plane plotted. Also, each of the remaining batches show uniform placement relative to the others for each plane of interest. The lowest volume fraction, 5% by volume, is the only batch of samples that tends towards the ideal operation location. In each plane of interest, the 5% volume fraction measures the highest degree of alignment and the largest normalized remanent magnetization.

Batches of samples with more than 5% by volume show relatively little variance in remanence magnetization, but a large variance in

calculated particle alignment. This suggests that increased volume content above 5% has little effect on increasing the effective remanent magnetization, however, the varied amount of magnetic material will have an effect on particle alignment. A large increase in particle alignment and little increase in remanent magnetization may suggest particle interactions or agglomerates may be limiting the bulk magnetization. This behavior may also indicate the formation of structures which have differential effects in alignment and magnetization.

The distribution parameter, measures the orientation of magnetic domains and the alignment parameter,  $\eta,$  measures the physical alignment of crystals in a sample. To determine if a correlation exists between the net magnetic orientation of a sample and the physical particle alignment of a sample each parameter is plotted with varied volume content.

It is expected a highly aligned sample will have greater bulk magnetization thus a small distribution of magnetic domains. For this criterion to be met, data points are expected to tend toward the lower right corner of each plot. Results show that the 5% by volume sample is the batch that most closely reaches the desired performance region. The 10% by volume batch is approaching the desired region as well. The 20% and 15% by volume samples show the lowest alignment and greatest distribution of magnetic domains.

A correlation observed in Fig. 12 is the behavior of the 20% and the

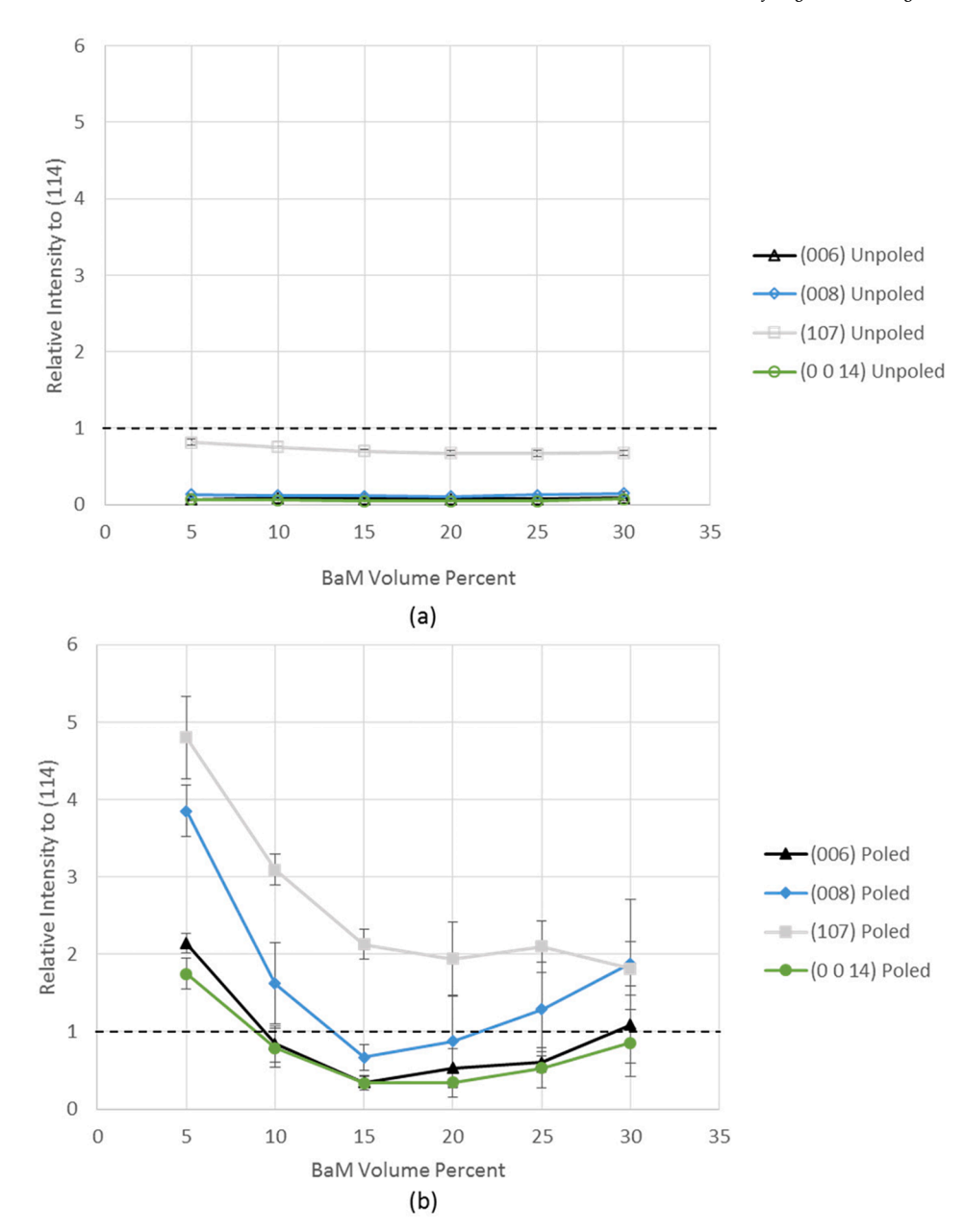


Fig. 9. Average relative intensity to the (114) peak of each batch of samples. (a) Shows unpoled samples and (b) shows poled samples. Note that the relative intensity of the (00 l) peaks for the poled samples is much higher than the relative intensity in the same plane for the unpoled samples. The dotted line shows the (114) relative intensity. Values above this line have larger absolute intensities than the (114) plane.

Table 1
Relative intensities of poled and unpoled samples with 80% confidence interval.

Relative Intensity to (114)								
Volume (%)	Poled Samples (006)	(008)	(107)	(0 0 14)	Unpoled Sample (006)	es (008)	(107)	(0 0 14)
5	$2.14\pm0.08$	$3.85 \pm 0.21$	$4.80\pm0.33$	$1.75\pm0.12$	$0.07\pm0.00$	$0.13\pm0.00$	$0.81\pm0.02$	$0.06 \pm 0.00$
10	$0.84 \pm 0.14$	$1.62\pm0.33$	$3.10\pm0.64$	$0.79 \pm 0.16$	$0.09\pm0.01$	$0.12\pm0.00$	$0.75\pm0.00$	$0.06\pm0.00$
15	$0.34\pm0.05$	$0.67 \pm 0.10$	$2.13\pm0.12$	$0.34 \pm 0.05$	$0.07\pm0.00$	$0.11\pm0.00$	$0.70\pm0.00$	$0.05\pm0.00$
20	$0.47\pm0.11$	$0.81\pm0.13$	$1.82 \pm 0.14$	$0.38 \pm 0.05$	$0.07\pm0.00$	$0.11\pm0.00$	$0.67\pm0.00$	$0.05\pm0.00$
25	$0.60\pm0.08$	$1.29\pm0.38$	$2.10\pm0.21$	$0.53\pm0.16$	$0.07\pm0.01$	$0.12\pm0.01$	$0.67\pm0.00$	$0.5\pm0.00$
30	$1.09\pm0.32$	$1.88\pm0.53$	$1.81\pm0.22$	$0.85\pm0.27$	$0.08\pm0.00$	$0.15\pm0.01$	$0.68 \pm 0.00$	$0.07\pm0.00$

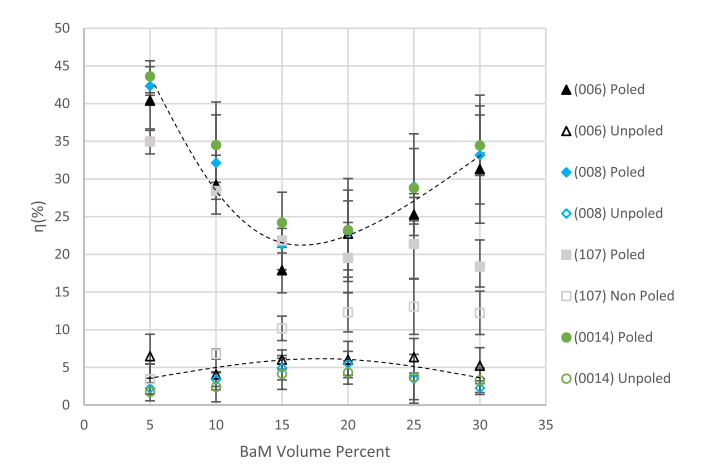


Fig. 10. Calculated degree of preferred orientation parameter,  $\eta$ , for each volume fraction. Solid data points represent poled samples, and hollow data points represent unpoled samples. Each data color represents an index plane of interest in the direction of poling. Dotted lines are drawn to show the trend in poled and unpoled batches.

30% by volume batches. Each of these batches have nearly the same average  $\sigma$  value, but the average  $\eta$  value shows variation. This trend suggests a greater alignment may not correlate with a more narrow alignment of magnetic domains. However, this phenomenon may be explained by considering the XRD measurements only capture a small spot size on the sample. The VSM measures the entire bulk sample magnetization. The XRD measurement may not capture enough of the sample to accurately describe the bulk material behavior. It is also important to note the XRD methods cannot distinguish the direction of the c-axis. The XRD techniques can determine if the c-axis is perpendicular to the sample surface but cannot differentiate whether the magnetic domain is aligned in the direction of poling or reversed. Having a large number of reversed domains will result in a high preferred alignment value but will greatly reduce the measured remanence magnetization. These reversed domains can be magnetically favorable since they close magnetic loops.

#### 3. Discussion of results

VSM results of poled samples show that the normalized remanent and highest achieved magnetization remains relatively constant for samples of 10%% volume and above, with the lowest, 5% sample having a higher value than the other compositions (see Fig. 5). Results also show that the metric of alignment of magnetic domains,  $\sigma$ , appears to scale with the squareness ratio (see Fig. 7) and shows more alignment 5% sample than all others (Fig. 6). In all cases, pre-curing increases the magnetic domain alignment (lowers  $\sigma$ ) and thereby increases remanent magnetization.

XRD results show that pre-curing also increases the metric of physical crystallite alignment, namely  $\eta$  increases for all volume fractions (see Fig. 10). However, when viewed across volume fractions, an evolution of  $\eta$  is seen. In poled samples  $\eta$  is minimized near 15% - 20% volume fraction while in un-poled samples  $\eta$  is maximized in the same range. The 5% poled sample shows the most alignment.

Based on the findings of this study, it appears increases in the magnetic actuation performance, and efficient use of MAE material in actuators, may be possible by using compositions below 10% v/v. The lowest, 5% v/v showed improvements in magnetic and physical alignment above higher volume fractions that resulted in higher remanent magnetization per unit volume magnetic material (See Fig. 11). NOE

that the magnetization of a body scales magnetic torque production along with the external field according to  $\tau = m \times H$ . Therefore increasing the magnetization per unit volume of magnetic material, as was shown at lower volume fraction herein, is beneficial in this instance because it allows use of less magnetic material for similar torque densities.

In contrast, increased MAE actuator performance may not be attainable solely by increasing volume fraction of magnetic material. This would be the case in MAE compositions 10% or greater in uses where the MAE actuator's effective composite stiffness varies linearly (or higher) with the volume of MAE material. Because the magnetization per unit volume magnetic material was shown to remain constant at and above  $10\% \, \text{v/v}$  (see Fig. 10), the constant value results in a linear scaling with increasing volume fraction that could be offset by increased material stiffness due to elastic reinforcement.

It should also be noted, in the general design of MAE actuators, that linear increase in thickness of bending MAE actuators, which scales actuator volume and therefore torque produced linearly, will generally be offset be the accordant change in elastic bending stiffness, which scales as the thickness cubed.

When comparing magnetic ( $\sigma$  from VSM) and physical ( $\eta$  from XRD) metrics of alignment, unexpectedly, results show that while the distribution of magnetic domains remains relatively constant, the degree of physical alignment still increases (see Fig. 12) . This somewhat confounding result suggests that as volume fraction is increased, structures develop that increase in physical alignment, but do not subsequently increase the alignment of magnetic domains in the remanent state.

A straightforward example explanation begins by considering stacks of particles (see Fig. 13a with plate-like particle shown on edge). Here, stacks are considered arrangements of successive particles layered on top of one another, with their out of plane easy axes aligned, examples of which can be see in in Fig. 3b. In other literature, these would be considered chains when successive stacks are aligned. Now consider two stacks of plate-like particles (See Fig. 13b-c). With the easy-axis shown out of the plane of the plate, individual stacks can have aggregate north and south poles as shown schematically given that, to first order, the constructive summation of the aligned dipole moments of individual particles. However, two stacks in proximity must seek a low energy state between themselves. This state can either be formed by a combined parallel collinear stack, or formed when the stacks align anti-parallel but adjacent to each other (see Fig. 13b-c). While less energetically favorable arrangements (oblique incidence) may occur, discussion is limited to the more favorable possibilities. The anti-parallel case is actually the lower energy state given the two dipole moments are anti-parallel such that, to first order, the summation of their aligned dipole moments is zero. See calculations of magnetic dipole-dipole interaction energies in Appendix B for more details.

It is further possible, that the degree of mobility, which arguably changes as we move from low volume fraction to higher volume fractions (approaching percolation) affects the degree of interaction of individual particles seeking to form multi-particle stacks, and of stacks seeking to realign to lower their overall magnetic energy density as they form multi-stack arrangements. For example, low volume fraction allows more mobility, thus multi-particle stacks may more easily form and align themselves with the external field, but these now aligned stacks may not be in close enough proximity to other aligned stacks for dipole–dipole interaction strong enough to overcome viscous effects. Too much space may exist between the dipolar entities. In this fashion, the low volume fraction may reduce occurrence of both the collinear and anti-parallel structures, yielding dispersed, multi-particle, but still physically well aligned, stacks as a result.

At high volume fraction, however, while dipole-dipole interactions

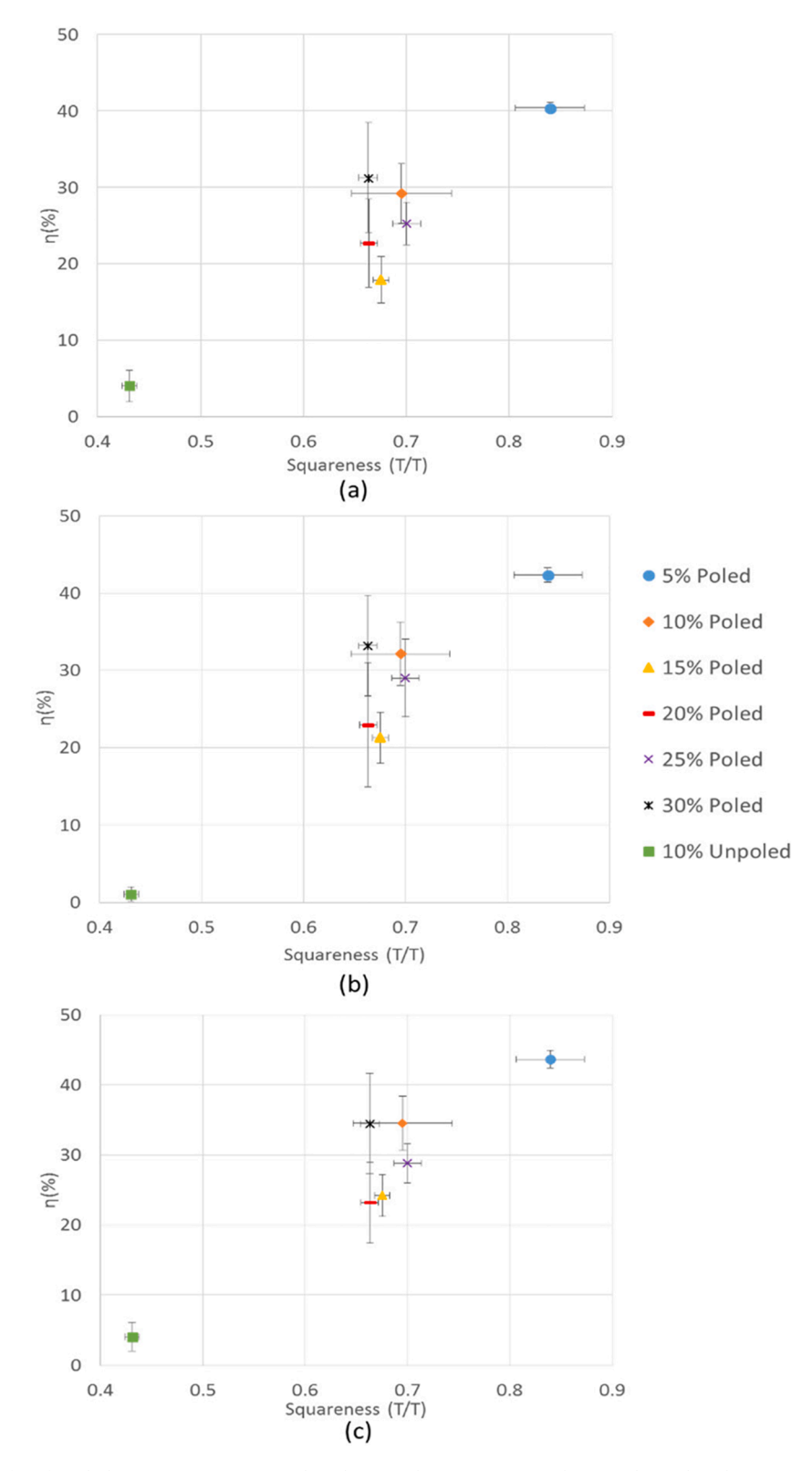


Fig. 11. Calculated degree of preferred alignment parameter,  $\eta$ , plotted versus the squareness to observe relationships between particle alignment and physical alignment for varied volume fractions. (a) Shows (006) alignment, (b) shows (008) alignment, and (c) shows (0 0 14) alignment.

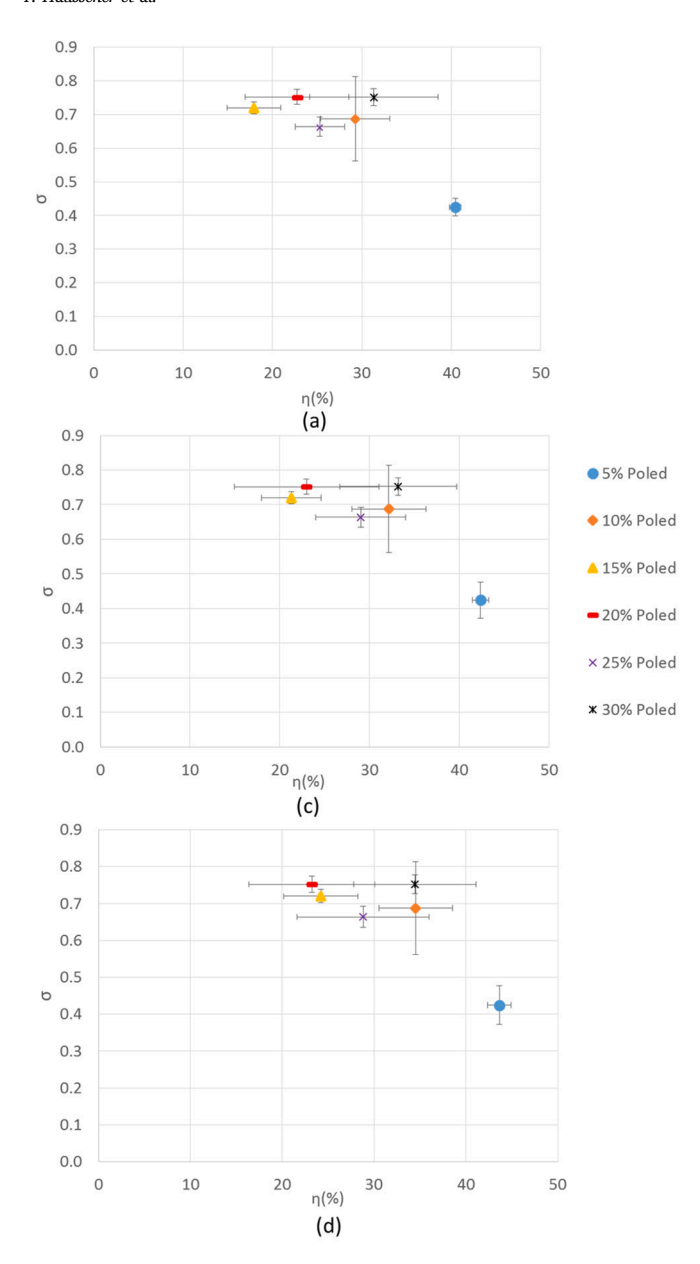


Fig. 12. Plots of the average calculated magnetic distribution parameter,  $\sigma$ , versus the average calculated degree of alignment parameter,  $\eta$ , for each batch. The error bars on each data point shows the standard deviation of each batch. (a) Shows alignment in the (006) plane, (b) shows alignment in the (008) plane, and (c) shows alignment in the (0014) plane.

will be stronger than at low volume fractions due to proximity, that proximity also reduces mobility through physical interaction. It is possible that while multi-particle stacks can form due to local proximity and dipole–dipole attraction, and subsequently align to some degree with an external field, further multi-stack alignment, collinear or antiparallel, may be reduced.

This mechanism would present the interesting possibility that there exist an *intermediate* volume fraction where multi-particle stacks may readily form in close enough proximity to each other for dipole interaction, while at the same time having enough space and mobility to form the lowest energy anti-parallel case. Note that the ideal anti-parallel case will register as increased physical alignment through XRD (given ideally parallel crystallites) but also as lower alignment through VSM (given

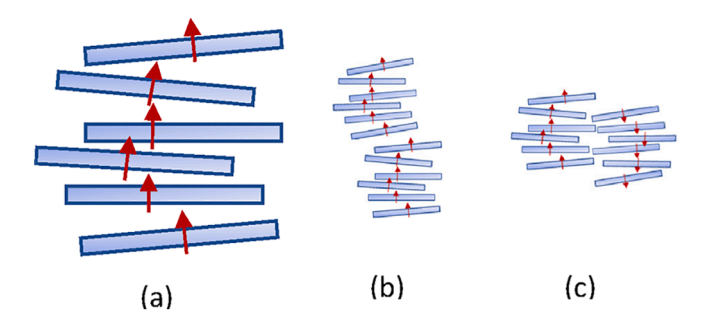


Fig. 13. Schematic a of possible multi-particle stack arrangements. (a) plate-like particles shown edge on (blue) align their easy axes (red) due to dipole—dipole interaction to form stacks, then either (b) stacks interact to form collinear structures to align aggregate dipoles, or (c) stacks align anti-parallel to form minimum energy structures.

opposing magnetic dipoles). This combination could result in the experimentally observed reduction in physical alignment at the intermediate 15%-20% volume fractions (see Fig. 10). The mechanism could also present as the observed lack of increase in magnetic alignment while physical alignment increases across volume fractions (see Fig. 12).

#### 4. Conclusions

This work studied the effect of increased barium hexaferrite composition as a magnetic filler material in magneto-active elastomers on physical particle crystallite alignment, magnetization orientation distribution, and bulk sample magnetization. Batches of MAEs were fabricated with BaM contents of 5%, 10%, 15%, 20%, 25%, and 30% by volume; each batch was divided into a sub-batch that was poled out-of-plane and a sub batch that was left unpoled.

Results showed that exposure to a magnetic field during curing increased physical and magnetic alignment as well as remanent magnetization, as expected. Results also suggest that the degree of physical and magnetic domain alignment evolves with volume fraction, promoting the highest physical and domain alignment at the lowest volume fractions. Results ultimately suggest that careful processing is needed to ensure effect utilization of the magnetic filler with low magnetic volume fractions ( $\sim 5\% \text{ v/v}$ ) possibly creating structures that promote higher magnetic remanence. More work studying composition increments at low volume fractions are suggested to track the evolution of the alignment response in this range. Further study of the behavior of materials with different crystal structures could also lead to insights on the evolution of structured formed and their effects on bulk properties versus volume fraction.

## **Funding**

We gratefully acknowledge the support of the National Science Foundation EFRI grant number 1,240,459 and the Air Force Office of Scientific Research. Any opinions, findings, and conclusions or recommendations expressed in this material are those of the author(s) and do not necessarily reflect the views of the National Science Foundation. We also acknowledge the funding from Penn State College of Engineering's ROCKET Seed Grant competition.

#### **Declaration of Competing Interest**

The authors declare that they have no known competing financial interests or personal relationships that could have appeared to influence the work reported in this paper.

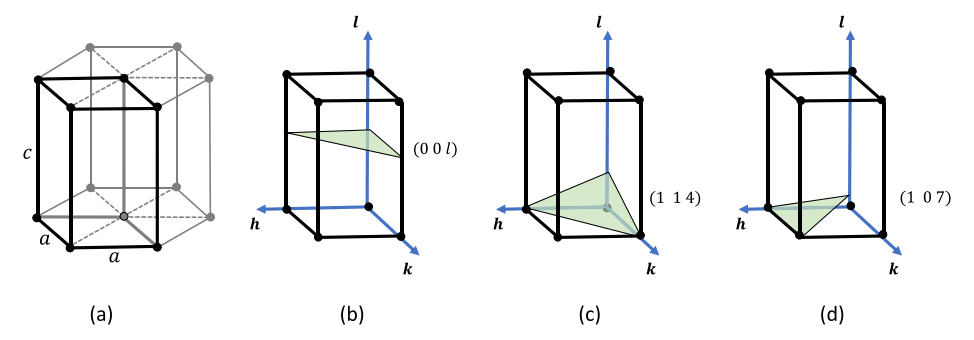


**Fig. A1.** Hexagonal crystal lattices. (a) Ideal crystallographic structure showing the two in-plane lattice parameters *a*, and the out-of plane parameter *c*, (b) (001) plane, (c) (114) plane and (d) (107) plane.

#### Appendix A

X-ray diffraction techniques utilize the scattering effects that occur when x-rays interact with the regular spacing and arrangements of atoms to produce identifiable and differentiable characteristic scattering patterns. These patterns occur when an emitter sends x-rays into a sample while a collector records the intensity of the scattered x-rays. The angle of incidence of the emitter and subsequent relative angle of the collector are important details, discussion of which is beyond the scope of this appendix(see reference [24] for further details).

For this work, a representative of each specific plane associated with our study of barium hexaferrite is shown in Fig. A1. Note that the studied planes include all successive planes associated with  $\{0,0,6\}$ ,  $\{0,0,8\}$ ,  $\{0,0,14\}$  and  $\{1,1,4\}$ , and  $\{1,0,7\}$  symmetries. The redundant fourth index has been omitted to align with the scattering results presented without loss of generality.

Consider that within a crystal region of similar orientation, each plane will scatter x-rays at a given intensity yielding a nominal XRD pattern at a nominal angle of incidence. However, across the distribution of orientations in a polycrystalline material or across particles of varying bulk orientation, the nominal scattering of the ideal crystal shifts when viewed with respect to some fixed axis, but still is self-consistent with respect to the relative orientations inside a given crystalline region. Specifically, each crystalline region will yield the idealized XRD pattern when excited at its own nominal angle of incidence which may differ from other crystalline regions in the sample. The March parameter, and the estimation of the degree of orientation that follows from it, account for the variation in distribution of the orientation of different crystalline regions within the spot size of the XRD machine. The result yields a metric of how uniformly aligned the crystalline regions are based upon comparison idealized XRD pattern of the pure material at the nominal angle of incidence versus the measured results across a range of incident angles [24]. Further details can be found in the reference, but are beyond the scope of this work.

### Appendix B

Arguments for the parallel and anti-parallel stack arrangements find their basis in two key elements:

- 1) the assumption that given barium hexferrite's hard-magnetic *c*-axis, which allows particles to be viewed individually as dipoles, aggregates of particles may further create an aggregated dipole, specifically having a local magnetization equivalent to the sum of the magnetic dipoles in the aggregate; and
- 2) the investigation of the potential energy between dipoles (either between individual particles or between stacks of particles) as given by

$$H = \frac{-\mu_0}{4\pi |\mathbf{r}|^3} (3(\mathbf{m}_1 \cdot \hat{\mathbf{r}})(\mathbf{m}_2 \cdot \hat{\mathbf{r}}) - (\mathbf{m}_1 \cdot \mathbf{m}_2))$$
(B1)

where  $m_1$  and  $m_2$  are the magnetization of either two individual particles or of two aggregates of particles, and r is the vector between dipole centers.

For the sake of analysis, consider the two dipoles defined in a 2D Cartesian system by

$$m_1 = m\left(\cos\theta_1\hat{i} + \sin\theta_1\hat{j}\right)$$
 (B2-a)

$$m_2 = m\left(\cos\theta_2\hat{i} + \sin\theta_2\hat{j}\right)$$
 (B2-b)

where m is the magnitude of the dipole (assumed equivalent for each dipole, particles with particle, or stack with stack), r = |r| and

$$\mathbf{r} = r\left(\cos\theta_r \hat{\mathbf{i}} + \sin\theta_r \hat{\mathbf{j}}\right) \tag{B3}$$

is the vector separating the centers of  $m_2$  and  $m_2$ . The dipoles are treated as ideal point dipoles for the this analysis.

Aggregates of particles that arise from argument 1 have the ability to enhance or diminish bulk magnetization. Fig. 13a depicts a well aligned aggregate of dipoles, herein called a *stack*, which to first order would have a magnetization *m* derived from the sum of the magnetizations of the individual particles contained in the aggregate, neglecting demagnetizing factors and assuming ideal magnetic behavior for sake of a simplified discussion as has been suggested elsewhere [26]. In a well aligned stack, the magnetization in the stack is enhanced by individual particle alignment. Fig. 13b depicts a case in which two aggregates are themselves aligned such that their net magnetization is enhanced. However, Fig. 13c depicts the opposite case, where the magnetizations of the two aggregates are in opposition such that the net magnetization is reduced. Moreover, in this opposing case a portion of the magnetic material would not contribute to the bulk magnetization, hence the total magnetization per unit magnetic mass would be decreased.

A rationale for the initial formation of well aligned stacks (Fig. 13a), and for the parallel (Fig. 13b) and anti-parallel (Fig. 13c) arrangement of stacks, is found in argument 2, examination of the potential energy between dipoles. Given equations (B2) and (B3), equation (B1) reduces to

$$H^* = -(3(\cos\theta_{1r})(\cos\theta_{2r}) - \cos\theta_{12})r^{-3}$$
(B4)

where  $\theta_{ab} = \theta_a - \theta_b$ , and  $H^* = (m^2 \mu_0 / 4\pi)^{-1}$ .

In the case where the dipoles, individual particles or stacks of particle, are collinear and parallel (Fig. 13b), eq. (B4) reduces to

$$H_{\parallel}^* = -2r^{-3}$$
 (B6)

where we see a minimum energy case when the dipoles form the collinear stack with  $r \rightarrow 0$  driving any subsequent reduction in energy. Hence, stack formation and alignment of stacks are promoted. This arrangement however, must still satisfy the divergence of the B field, namely

$$\int \nabla \cdot \mathbf{B} = 0 \tag{B7}$$

which requires the return of magnetic flux from the north end of a stack to the south through air, a high magnetic impedance medium. The anti-parallel case helps address the divergence issue by lowering the magnetic impedance while still offering a low energy state.

Consider stacks as dipoles where two are anti-parallel and adjacent (Fig. 13c) which reduces equation (B4) to

$$H^* = -r^{-3}$$
 (B7)

where the potential energy may be further reduced by decreasing r. While the energy is higher than the collinear and parallel case, the pair provide a framework for understanding how a series of stacks encompassing an arc of  $360^{\circ}$  can aid completion of the magnetic flux path needed to satisfy the divergence requirement by creating a lower impedance route from north back to south poles. Along this arc, any two adjacent stacks will have their energy bounded by either  $H^* = -2r^3$  if the pair form a shallow arc  $(\theta_{1r} \to 0)$  or  $H^* = -r^3$  if the pair approach anti-parallel  $(\theta_{1r} \to -\pi)$ , the two extremes of Fig. 13b-c, respectively. Consequently, the anti-parallel case, or a more complex closed loop, may lower the magnetic impedance, have favorable energy dipole energy characteristics between adjacent stacks, while providing no additional magnetization to the bulk from the magnetic material in the loop. This response mirrors what has been seen experimentally in this work.

#### Appendix C

The width of the distribution  $\sigma$  was found by fitting the experimentally measured squareness,

$$S_{exp} = \frac{M_{i}}{M}$$

where  $m_r$  is the remanence and  $M_s$  the nominal saturation (here is average highest recorded magnetization), to the squareness values predicted by a Gaussian distribution of magnetic domain alignment [20]. The prediction method assumes each domain exists at remanence at some orientation  $\phi$  such that the width of the distribution about  $\phi = 0$  gives a metric of the degree of alignment. The predicted value is given by

$$S_{pred} = \frac{1}{N_f} \int_0^{\pi/2} f(\phi | \sigma^2) |\cos\phi| \sin\phi d\phi$$

where

$$f(\phi) = \frac{1}{\sigma \sqrt{\pi}} e^{-\frac{\phi^2}{2\sigma^2}}$$

and the normalizing factor is given by

$$N_f = \int_0^{\pi/2} f(\phi) sin(\phi) d\phi$$

#### References

- Ginder, J.M., et al. Magnetorheological elastomers: properties and applications. in Smart Structures and Materials 1999: Smart Materials Technologies. 1999.
   International Society for Optics and Photonics.
- [2] J. Ginder, et al., Magnetostrictive phenomena in magnetorheological elastomers, Int. J. Mod Phys B 16 (17n18) (2002) 2412–2418.
- [3] X. Zhang, et al., Analysis and fabrication of patterned magnetorheological elastomers, Smart Mater. Struct. 17 (4) (2008), 045001.
- [4] A.A. Zainudin, et al., Rheological and resistance properties of magnetorheological elastomer with cobalt for sensor application, Applied Sciences 10 (5) (2020) 1638.
- [5] A. Hooshiar, A. Alkhalaf, J. Dargahi, Development and assessment of a stiffness display system for minimally invasive surgery based on smart magneto-rheological elastomers, Mater. Sci. Eng., C 108 (2020), 110409.
- [6] S. Sun, J. Yang, T. Yildirin, H. Du, G. Alici, S. Zhang, W. Li, Development of a nonlinear adaptive absorber based on magnetorheological elastomer, J. Intell. Mater. Syst. Struct. 29 (2) (2018) 194–204.
- [7] von Lockette, P. and R. Sheridan. Folding Actuation and Locomotion of Novel Magneto-active Elastomer (MAE) Composites. in Conference on Smart Materials, Adaptive Structures and Intelligent Systems. 2013. Snowbird, UT.
- [8] G.Y. Zhou, Complex Shear Modulus of a Magnetorheological Elastomer, Smart Mater. Struct. 13 (5) (2004) 1203–1210.
- [9] A. Boczkowska, et al., Image analysis of the microstructure of magnetorheological, J. Mater. Sci. (2009) 3135–3140.

- [10] P. von Lockette, et al., Investigating new symmetry classes in magnetorheological elastomers: cantilever bending behavior, Smart Mater. Struct. 20 (10) (2011).
- [11] J.-H. Koo, A. Dawson, H.-J. Jung, Characterization of actuation properties of magnetorheological elastomers with embedded hard magnetic particles, J. Intell. Mater. Syst. Struct. 23 (9) (2012) 1049–1054.
- [12] M. Radwan, M. Rashad, M. Hessien, Synthesis and characterization of barium hexaferrite nanoparticles, J. Mater. Process. Technol. (2007) 106–109.
- [13] R. Nowosielski, R. Babilas, J. Wrona, Microstructure and magnetic properties of commercial barium ferrite powders. Journal of Achievements in Materials and Manufacturing, Engineering 20 (1–2) (2007).
- [14] M. Sharma, et al., Enhancement of Curie temperature of barium hexaferrite by dense electronic, AIP Adv. 4 (7) (2014).
- [15] A. Wise, et al., M-type barium hexaferrite synthesis and characterization for phase shifter applications, J. Appl. Phys. 109 (2011).
- [16] D. Lisjak, S. Ovtar, The Alignment of Barium Ferrite Nanoparticles from Their Suspensions in Electric and Magnetic Fields, The Journal of Physical Chemistry 117 (2012) 1644–1650.
- [17] K. Martirosyan, et al., Barium hexaferrite nanoparticles: Synthesis and magnetic properties, Material Science and Engineering B 176 (2011) 8–13.
- [18] K. Sadhana, K. Praveena, S. Matteppanavar, Structural and magnetic properties of nanocrystalline BaFe12O19 synthesized by microwave-hydrothermal method, Applied Nanoscience (2012) 247–252.

- [19] X. Jing, X. Shen, H. Song, Magnetic and dielectric properties of barium ferrite fibers/poly(vinylidene fluoride) composite film, J. Polym. Res. 18 (6) (2011) 2017-2021.
- [20] C. Breznak, P. von Lockette, Evolution of the Magnetization Response of Magneto-Active Elastomers Made With Hard-Magnetic M-type Barium Hexaferrite Particles, MRS Adv. 1 (1) (2016) 39-43.
- [21] H.S. Shin, S.-J. Kwon, A Suggestion on the Standard X-Ray Powder Diffraction Pattern of Barium Ferrite, Powder Diffr. 7 (4) (1992) 212–214.
- [22] x-ray Basics. Materials Research Laboratory at UCSB: An MRSEC, 2016.
- [23] K. Iwai, T. Kohama, Alignment Behavior of Bismuth Particles in Viscous Liquid under Imposition of Magnetic Field, Journal of the Japanese Society for Experimental Mechanics 12 (1) (2012) 33-36.
- [24] H. Klung, L. Alexander, X-Ray Diffraction Procedures: For Polycrystalline and Amorphous Materials, Wiley-Interscience, 1974.
- [25] E. Zolotoyabko, Determination of the degree of preferred orientation within the March-Dollase approach, J. Appl. Crystallogr. 42 (3) (2009) 513–518.

  [26] T.B. Jones, Electromechanics of Particles, Cambridge University Press, 1995.